SMF-MMF-SCF-Based Humanoid-Shaped Fiber-Optic Sensor for Wide Range of Magnetic Field Detection

Qianyun Yin, Ragini Singh, Yiran Wang, Bingyuan Zhang, and Santosh Kumar, *Senior Member, IEEE*

***Abstract*—In this study, we propose a fiber-optic magnetic field sensor based on a humanoid fiber structure. Considering that conventional magnetic field sensors are susceptible to electromagnetic interference, in this study we employed a fiber optic fusion splicer and a combiner manufacturing system (CMS) to fabricate a single-mode fiber (SMF), a multimode fiber (MMF), and a seven-core fiber (SCF) fused humanoid fiber optic sensor. Also, this study measured the magnetic field strength by coating the fiber optic sensing region with nickel ferrate ($NiFe_2O_4$) and using the ferromagnetic nature of nickel group compounds. We performed a series of additional tests to assess the sensitivity, accuracy, and reproducibility of our fabricated humanoid fiber structure. Various experimental tests demonstrated that the sensitivity and accuracy of the humanoid fiber optic sensors were 1.1 pm/mT and 0.957, respectively, in an increasing magnetic field, and 0.5 pm/mT and 0.9619, respectively, in a decreasing magnetic field. The magnetic field sensor has proven to be very precise, capable of real-time monitoring, compact in size, and able to measure with minimal loss. As a result, the magnetic field sensor is highly advantageous in healthcare monitoring and geological surveys because of its exceptional accuracy, real-time monitoring capability, compact size, and noninvasive measurement.**

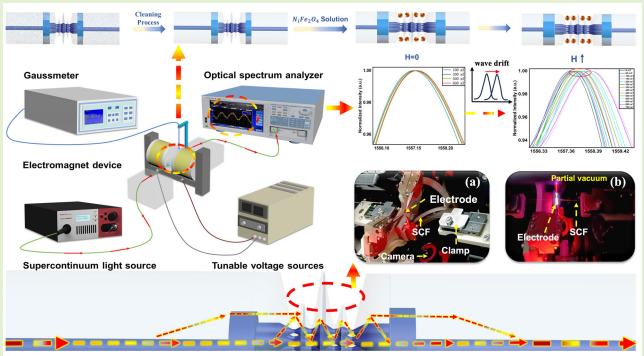

***Index Terms*—Evanescent wave (EW), fiber optic sensor, humanoid fiber structure, magnetometer, nickel ferrate ($NiFe_2O_4$).**

I. Introduction

FIBER optic sensing technology is advancing at a rapid pace, and its key benefits—including high sensitivity, robust anti-interference ability, good insulation performance, digitization capability, high reusability, and dynamic measurement—indicate that it will play a major role in magnetic field sensors in the future. High-performance fiber-optic magnetic field sensors, with their lightweight, miniaturized design, remote manipulation capabilities, and real-time monitoring functions, are particularly useful in the detection of electromagnetic systems [1], [2], geologic exploration [3], [4], biomedical imaging [5], [6], [7], [8], [9], and other fields. The magnetic field sensors are essential to many scientific research projects and engineering applications. In recent years, optical fiber magnetic field sensors using magnetic nanoparticles to immobilize the sensing area have been reported [10]. At the same time, different fiber optic structures have been designed for the measurement of magnetic field strengths, depending on the magnetic field measurement range. Sharma et al. [11] developed a tapered fiber optic magnetic field sensor capable of detecting magnetic fields ranging from 0 to 200 mT. Conventional magnetic field sensors rely on the principles of electromagnetism and when the external magnetic field undergoes a change, the detection signal becomes highly susceptible to interference from the external magnetic field, thereby becoming unstable [12]. This interference can have a major impact on the accuracy of magnetic field measurements.

Manuscript received 26 April 2024; revised 31 May 2024; accepted 1 June 2024. Date of publication 10 June 2024; date of current version 16 July 2024. This work was supported in part by the Double-Hundred Talent Plan of Shandong Province, China; in part by Liaocheng University under Grant 318052341; in part by the Special Construction Project Fund for Shandong Province Taishan Mountain Scholars; and in part by the Science and Technology Support Plan for Youth Innovation of Colleges and Universities of Shandong Province of China under Grant 2022KJ107. The associate editor coordinating the review of this article and approving it for publication was Dr. Sanjeev Kumar Raghuwanshi. *(Corresponding authors: Yiran Wang; Santosh Kumar.)*

Qianyun Yin is with Ji Xianlin College and School of Physics Science and Information Technology, Liaocheng University, Liaocheng 252059, China (e-mail: 2316334238@qq.com).

Ragini Singh is with the Department of Biotechnology, Koneru Lakshmaiah Education Foundation, Vaddeswaram, Andhra Pradesh 522302, India (e-mail: raginisingh@kluniversity.in).

Yiran Wang and Bingyuan Zhang are with Shandong Key Laboratory of Optical Communication Science and Technology, School of Physics Science and Information Technology, Liaocheng University, Liaocheng 252059, China (e-mail: wangyiran6717@163.com; zhangbingyuan@lcu.edu.cn).

Santosh Kumar is with the Centre of Excellence for Nanotechnology, Department of Electronics and Communication Engineering, Koneru Lakshmaiah Education Foundation, Vaddeswaram, Andhra Pradesh 522302, India (e-mail: santosh@kluniversity.in).

Digital Object Identifier 10.1109/JSEN.2024.3409508

The sensor's sensitivity can result in significant variations in its performance across different settings, thereby affecting the accuracy and consistency of the measurement data. Traditional magnetic field sensors may struggle to ensure consistent and precise data in dynamic electromagnetic environments, leading to challenges in data repeatability and accuracy. To address these challenges, it is imperative to promptly design a novel type of fiber-optic sensor.

One point that cannot be ignored is that at this stage, fiber optic magnetic field sensors are still facing a number of difficulties, e.g., the magnetic fluid used in conventional magnetic field sensors solidifies over time, which makes it difficult for magnetic fluid to redistribute on the surface of the optical fiber, and thus leads to the deterioration of the detection performance of the magnetic field sensors. During our experiments, we fabricated a nickel ferrate ($NiFe_2O_4$) coating on the tapered cross section as the sensing element of the humanoid electromagnetic sensor in the hope that the material can overcome this difficulty. The sensor utilized optical fibers that were connected by single-mode optical fiber-multimode optical fiber-seven core optical fiber (SMS) fusion splicing. We used $NiFe_2O_4$ over cladding of the humanoid fiber optic sensor's sensing region, taking advantage of the phenomenon of magnetic domains [13], [14], [15] in the magnetic field characterized by $NiFe_2O_4$. By varying the magnetic field's strength, we were able to alter the arrangement of $NiFe_2O_4$, which in turn changed the wavelengths that corresponded to wave peaks in the optical spectrum analyzer (OSA).

The experiment aims to conduct a comprehensive examination of the evanescent wave (EW) in the humanoid fiber structure and reproduce it by leveraging the structure's portability, resilience, economy, and usefulness. Total internal reflection occurs when light propagates from an interface with a high refractive index (RI) to an interface with a low RI. For total internal reflection, the Fresnel coefficient of the transverse wave is not zero, which leads to the fact that when total internal reflection occurs, a portion of the light wave propagates into the low RI medium and decays exponentially with distance from the surface, and this wave field is called an EWs [16]. Before selecting the humanoid optical design for the development of the optical magnetic field sensor in the fabrication of the fiber optical probe, we thoroughly evaluated the pros and cons of the various fiber optic structures currently available in the market. The fusion splicing technique was used to obtain the SMS fiber structure during the experiment. Subsequently, the humanoid fiber structure is attained through the configuration of the combiner manufacturing system's (CMS) parameters. Real-time magnetic field monitoring is achieved by adjusting the current of the adjustable voltage supply to vary the magnetic field surrounding the probe during the investigation. The magnetic gradient within the monitoring zone of the optical fiber is measured using a Gaussmeter. To evaluate the response time and real-time monitoring capabilities of the magnetic field's sensor, we altered the magnetic field strength around the instrument's probe during the experiment by adjusting the current of the power supply. Subsequently, we employed an automatic Gaussmeter to measure the magnetic field within the detection segment of the optical fiber.

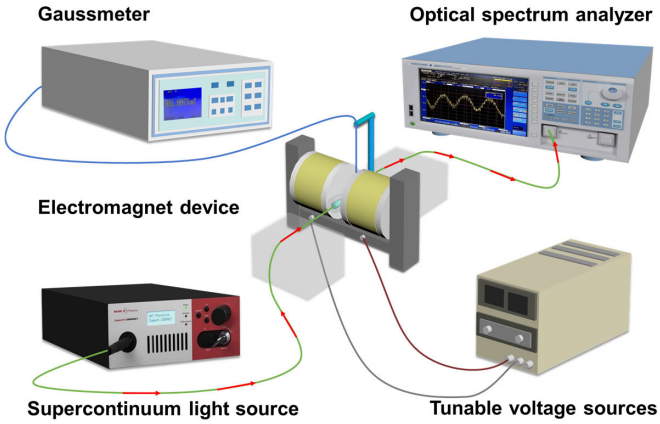

Fig. 1. Experimental setup for magnetic field measurement using humanoid-shaped optical fiber sensor.

II. Experimental Section

A. Materials and Instrument

Fig. 1 illustrates the experimental configuration utilized in this technique to assess the fiber optic sensing probe's characterization properties. We primarily obtained the single-mode fibers (SMFs), multimode fibers (MMFs), and seven-core fibers (SCFs) used in this experiment from Shenzhen Ebolink Technology Company, China. The instruments used in this experiment include an electromagnet device (Shanghai Huayan Instrument Company Ltd., Shanghai, China) for producing variable magnetic fields, a supercontinuum light source (SUPERK COMPACT, NKT Photonics, 450–2400 nm), an OSA (AQ6370D, YOKOGAWA, 600–1700 nm), a Gaussmeter (CH-1800, CH-Magnetoelectricity Technology) [17], and a tunable voltage source for producing variable magnetic fields. We fixed the optical fiber using two fiber optic clamps on both sides of the experimental apparatus to guarantee that the optical probe's position in the magnetic field would not change throughout the experiment. We used a stopwatch to make sure the optical fiber's action time in the magnetic field remained constant, and we made sure the entire experiment was conducted at room temperature (26 °C) to minimize the impact of the outside environment on the magnetic field measurement data. To further assure the validity and real-time nature of the measurement results, a Gaussmeter probe is positioned close to the optical probe to measure the magnetic field surrounding the investigation in real time. Throughout the experiment, the strength of the magnetic field surrounding by adjusting the voltage of the tunable voltage source, and the strength of the magnetic field around the fiber optic instrument is changed during the experiment.

It is important to remember that when using a humanoid fiber structure with $NiFe_2O_4$ as the coating for magnetic field measurements, the impact of the concentration of $NiFe_2O_4$ on the probe's sensitivity needs to be taken into account. As the stacking of nanoparticles increases during the process of detecting the magnetic field, the change in the RI of the nanomaterial becomes stronger.

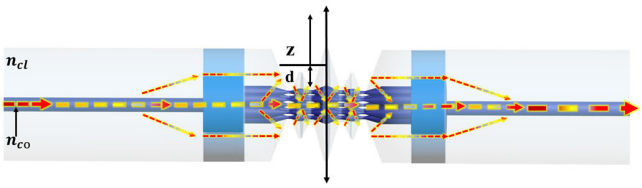

Fig. 2. Optical signal propagation through humanoid fiber optic structure.

After considering the measurement impact, relevant material properties, and the cost of producing the structure, we ultimately chose to use $NiFe_2O_4$ with a concentration of 1 mg/mL as the coating material for this experiment.

B. Sensing Principle

Magnetic particles are able to display the unique phenomenon of magnetic domains in magnetic fields, i.e., when the magnetic particles are positioned in a magnetic field, the structure of the microscopic objects that possess electromagnetic in the magnetic particles varies with the intensity and direction of the magnetic field. The magnetic field causes magnetic particles to aggregate into chains along its direction. As the power of the magnetic field changes, so does the degree of chaining of magnetic particles. This causes variations in the RI of the light beam passing through the magnetic material and, as a result, the magnetic nanomaterials in the magnetic field, which causes the wave peaks on the OSA to drift [17].

The dielectric magnetization (χ_e) of $NiFe_2O_4$ in the sensing region is altered by an external magnetic field (H), and this alteration affects the RI of the magnetic nanoparticles. In turn, the electromagnetic properties of the magnetic nanoparticles are specifically correlated with its RI, which can be represented by the following equation [12], [18]:

$$\eta_{NiFe_2O_4} = \sqrt{\varepsilon_{NiFe_2O_4}} = \sqrt{1 + \chi_e}. \tag{1}$$

The optical fibers used in the experiment are composed of core and cladding with different RI. When the optical signal is transported from an SMF to an MMF, less light energy is lost. Light propagates from the core to the cladding in the fusion splice region of an MMF and an SCF very easily because MMF can transmit more transmission modes and have a core diameter that is larger than an SCF core. A portion of the light will simultaneously propagate from the core to the cladding in the tapered-shaped humanoid fiber optic sensor, forming an EWs. This portion of the light will then return to the core via the coated ferromagnetic material. The depth of penetration of the EWs in the cladding can be expressed as follows [19], [20]:

$$d_p = \frac{\lambda}{2\pi\sqrt{n_{\text{co}}^2 \sin^2\theta_i - n_{\text{cl}}^2}}. \tag{2}$$

As seen in Fig. 2, the EWs light intensity decays exponentially in the area of optical detection's z-axis, with the following equation:

$$I_z = I_0 e^{-\frac{d}{z}}. \tag{3}$$

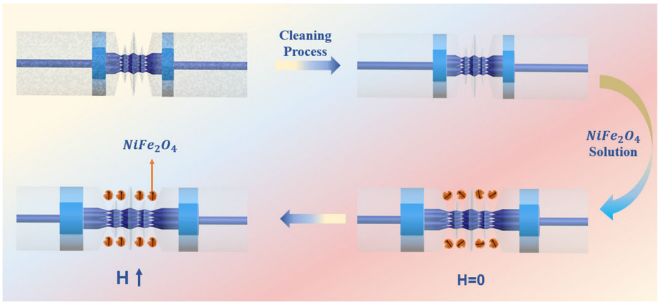

Fig. 3. $NiFe_2O_4$ coating process over humanoid-shaped fiber optic structure.

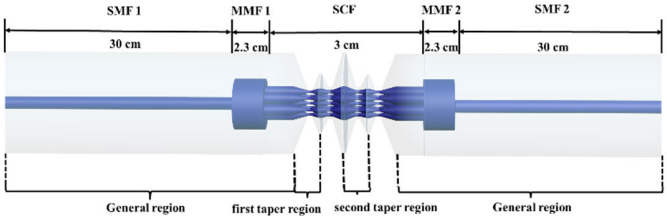

Fig. 4. Schematic of humanoid optical fiber structure.

Furthermore, as illustrated in Fig. 3, $NiFe_2O_4$ coated on the optical fiber to enhance the humanoid fiber optic sensor's sensing capability. Due to the magnetic phenomenon of ferromagnetic materials like $NiFe_2O_4$, when the EWs pass through it, the RI of the magnetic nanoparticles changes. This alters the angle of deflection of the optical fiber and causes the spectral wave peak that the spectrometer detects to drift. The structural advantages offered by the humanoid fiber structure, on the other hand, can enhance the contact area between the light and the magnetic nanomaterials.

C. Simulation of Sensor Probe

We have simulated a novel humanoid fiber optic structure using the BeamPROP algorithm via RSoft software to understand the sensing performance of the structure and to model its fast field dispersion.

BeamPROP is an industry-leading design tool based on the beam propagation method (BPM) for designing and simulating integrated fiber optic waveguide devices and circuits. Superior robust and efficient results via an implementation of the BPM based on an implicit finite-difference scheme. Initially, the RSoft CAD module is used to simulate the designed humanoid fiber structure. The modeling process's pertinent parameters are set to match those of the actual optical fiber to guarantee the simulation findings' authenticity and accuracy. In this experiment, we used a 50 cm SMF with a 125 μm cladding diameter and an 8.2 μm core diameter. The MMF has a length of 2.3 cm, consisting of a 125 μm cladding and a 62.5 μm core. The length of the SCF is 3 cm, consisting of 6.1 μm for the core and 125 μm for the cladding, as shown in Fig. 4.

The central wavelength of incident light propagating in free space is 1.55 μm, and we employ a background RI of 1 in the simulation process. Fig. 5 shows the results of the simulation of the humanoid fiber structure in the xz plane using RSoft. Where 1, Launch denotes the total energy distribution of the light source incident on the core. 2, mode 0 denotes the energy

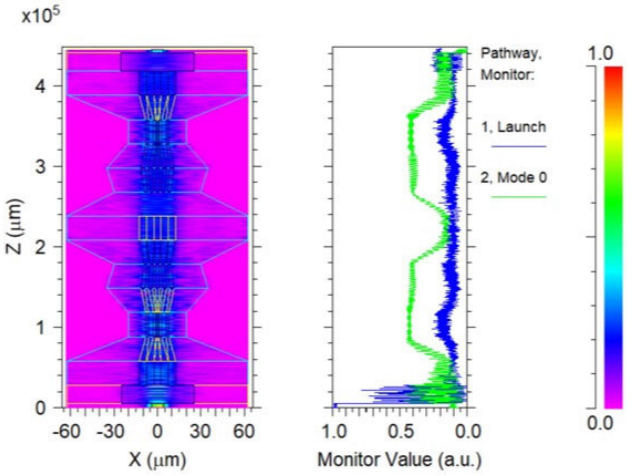

Fig. 5. Estimation of EWs and propagation modes of humanoid fiber structure.

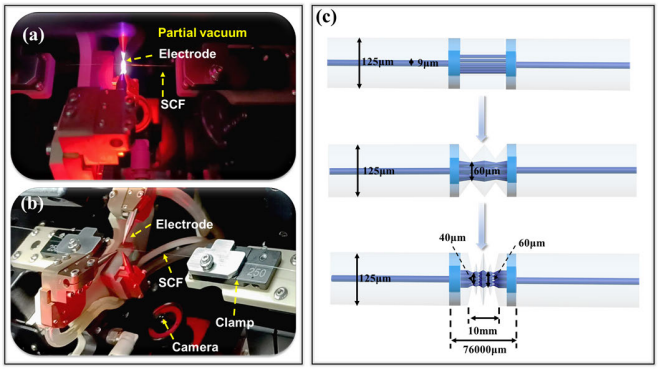

Fig. 6. (a) Internal schematic of the CMS. (b) Three electrodes' discharge procedure. (c) Fabrication steps of humanoid optical fiber structure.

distribution of the propagation modes of the humanoid fiber structure within the cladding. The RI shift causes the energy in the core to shift transitioning between the cladding and core dissemination modes when light enters the humanoid fiber sensing region, as shown in Fig. 6. Part of the light is scattered from the cladding to the air. This part of the light proceeds to be transmitted into the cladding after interacting with the ferromagnetic material in the sensing region. There, it experiences refraction and reenters the fiber core, enhancing its energy. According to the simulation results, the humanoid fiber structure can stimulate sturdy cladding modes. It also facilitates the generation of EWs and expands the beam's surface area in contact with the ferromagnetic material.

D. Fabrication of Sensing Probe

In this experiment, an SMF-MMF-SCF-based fiber structure is utilized. This fiber structure is heated by a plasma heating system for the construction of a humanoid fiber structure. The heated plasma is converted into a "thermally stabilized plasma" at the proper temperature by varying certain parameters in the computer system, such as the initial heating power and the cone heating power. When compared to other fiber optic production methods currently in use, this technology exhibits greater temperature stability. The uniform distribution of the thermally stabilized plasma around the electrodes renders the heating temperature of the fiber manufacturing system independent of various factors like electrode aging and wear and tear. This effectively mitigates the influence of both internal and external system factors on the repeatability of the fiber structure. The thermally stabilized plasma remains incredibly stable in a vacuum environment.

An overview of using CMS to fabricate a humanoid fiber structure is shown in Fig. 6. The three different types of fibers are fused together using electrode discharges in a fusion splicer after ordinary MMF, SMF, and SCF fibers have had their coatings removed. After that, the fused fiber optic structure is enclosed in a CMS, which uses a vacuum pump to generate a semi-vacuum working environment around the fused SMS structure in accordance with air pressure theory. The three electrodes will discharge uniformly, creating a homogeneous plasma field on the fiber surface, once the surrounding vacuum exceeds a set threshold. As the fiber heats up, the fiber moves on both sides uniformly, as seen in Fig. 6(a) and (b). The reproducibility of the fiber optic probes is increased when the fiber optic structures are prepared in this manner. During the experiment, a 60 μm taper region was first obtained on the SCF by optimizing the computer program. From there, two symmetrical 40 μm tapered structures were obtained in the 60 μm tapered by moving the z-axis [17] respectively, to form a complete humanoid fiber structure, as shown in Fig. 6(c). Upon completion of the taper pulling procedure, the monitoring system included within the CMS may produce a 2-D image of the fabricated fiber, enabling us to do an initial assessment and confirmation of the fiber structure's repeatability.

III. Results and Discussion

A. Characterization of Nanomaterials

$NiFe_2O_4$ is a substance having an anti-spinel structure and two metal elements: nickel and iron. In addition to having strong magnetic induction compressive strength and high magnetic energy product at saturation state, it also possesses superior heat resistance and magnetic conductivity. The electromagnetic characteristics of bimetallic oxides are better than those of monometallic oxides because the presence of two cations in a bimetallic oxide contributes more to active sites than in a single metal oxide. This experiment uses $NiFe_2O_4$-NPs that show exceptional electromagnetic capabilities in a magnetic field. The multicavity structure of $NiFe_2O_4$ improves the scattering and reflecting sites of electromagnetic waves. In the meantime, $NiFe_2O_4$ is a soft magnetic substance that is frequently employed. It has several uses, including magnetic and microwave-absorbing materials. $NiFe_2O_4$, one of the most significant soft magnetic materials with a spinel structure, is used extensively in electronic devices, information storage, magnetic resonance imaging, drug delivery, and other fields [21]. Its benefits include small coercivity and high saturation magnetization strength. Its large specific surface area, good ferromagnetic characteristics, low toxicity, high-performance stability, and biosafety make it a promising material for use in medical targeted materials,

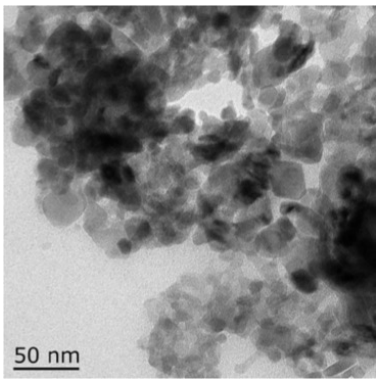

Fig. 7. HR-TEM image of $NiFe_2O_4$ nanomaterials.

catalysts, magnetic nanoparticles, and other applications. The important property of adjustable RI compared to other magnetic nanoparticle materials, as well as the fact that $NiFe_2O_4$ particles of different diameters exhibit different characteristics of paramagnetism and ferromagnetism under magnetic field conditions, making them the material of choice for magnetic field measurements [22].

To assess the relevant performance of the optical probe in rising and falling fields, we coated the humanoid fiber optic sensing region in this work with $NiFe_2O_4$ to develop an optical probe for a fiber optic magnetic field sensor. The instrument is surrounded by a magnetic field in this configuration, which can be adjusted via a tunable voltage source. Because of the excellent ferromagnetic characteristics of $NiFe_2O_4$, significant domain phenomena arise as the magnetic field strength varies, resulting in a change in the RI around the probe.

A spectrometer can be used to record the drift of the transmission spectrum's wavelength peaks. Fig. 7 shows an image of $NiFe_2O_4$ observed using a transmission electron microscope (HR-TEM, Talos L120C, Thermo Fisher Scientific, USA). The scanned TEM pictures clearly show the particles of $NiFe_2O_4$.

The original view of tapered sections in the humanoid fiber sensing region is observed using a scanning electron microscope (SEM) and depicted in Fig. 8(a). The illustration makes it evident that the fiber sensing region is divided into two symmetric tapering parts, measuring 40 and 60 μm, respectively. The fiber sensing zone's specific surface area can be increased by this construction, improving the magnetic nanoparticles' ability to adhere to the fiber sensing region. This establishes a solid basis for the humanoid fiber sensor to further demonstrate superior performance in detecting magnetic fields. Fig. 8(a) and (b) demonstrates the distribution of $NiFe_2O_4$ at different sensing locations. As shown in Fig. 8(b), $NiFe_2O_4$ is relatively uniformly distributed in the sensing region of the magnetic field sensor. The energy dispersive X-ray Spectroscopy (EDX) of the probe revealed the presence of $NiFe_2O_4$ at the fiber optic sensing region. It has a considerable amount of oxygen and iron and nickel components, as shown by the results in Fig. 8(c). This demonstrates that the immobilization of $NiFe_2O_4$ on the probe surface is successful. Since, silica makes up the majority of the fiber, the energy spectrum also shows evidence of elemental oxygen and silica.

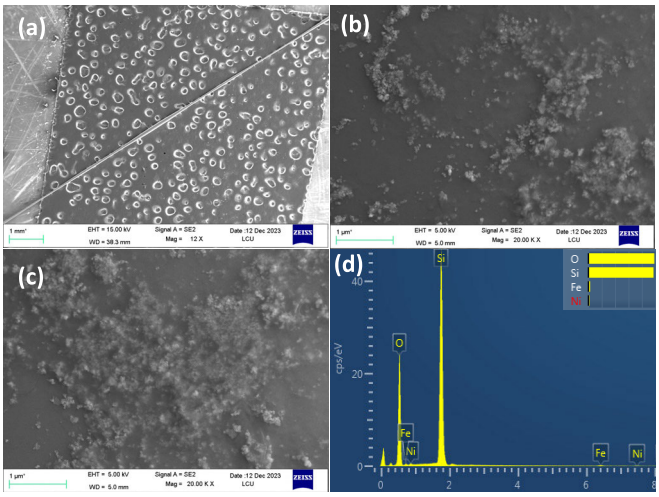

Fig. 8. (a) SEM image of humanoid bare fiber structure. (b) and (c) Distribution of $NiFe_2O_4$ at various sensing area of humanoid fiber optic sensor. (d) EDX image of $NiFe_2O_4$-coated fiber optic sensor probe.

B. Optimization of Sensor Structure

Based on the inspection of the spectrometer scanned images in Fig. 9(a), the SCF structure was selected for magnetic field strength measurements in this experiment. As can be seen from the figure, the use of an SCF during the fusion splicing process is able to monitor more transmission peaks in the transmission spectrum. Since in this experiment, we realized the magnetic field measurement by observing the drift of the peak wavelength, more transmission peaks allow us to observe the change more clearly in the OSA. At the same time, we guess that in the process of pulling the taper of the probe region, compared with the four-core fiber (FCF), SCF due to the core is closer together, the light in the sensing region is easier to achieve coupling in the taper region of the SCF. This allows the OSA to detect a greater intensity of transmitted light, reducing the coupling loss of light in the sensing region. A great degree of consistency can be observed in the humanoid-shaped fiber structure developed with CMS, as shown in Fig. 9(b). In the meantime, Fig. 9(c) demonstrates the great repeatability of the transmission spectrum peaks, ensuring the accuracy of the experimental results and reducing the possibility of mistakes resulting from modifications in the experimental environment. As depicted in Fig. 9(d), the transmitted light intensity of the $NiFe_2O_4$-coated humanoid fiber structure is less intense than the transmission spectrum intensity before coating, suggesting that the $NiFe_2O_4$ coating employed in this experiment has good sensing properties.

C. Magnetic Field Measurement

The uncoated fiber structure has inadequate sensitivity and accuracy under incremental magnetic field, as shown in Fig. 10. In addition, considering the possible impact of the external environment on the sensor performance, the uncoated humanoid fiber structure exhibits poor sensing capability in the incremental magnetic field. The findings displayed in Fig. 11 demonstrate that the transmission spectral wave peaks recorded by the spectrometer with decreasing magnetic field strength did not exhibit the desired drift in the uncoated

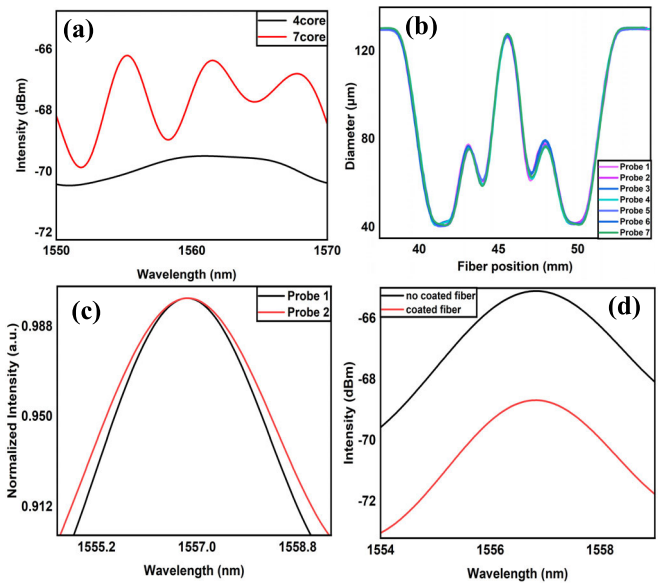

Fig. 9. (a) Transmission spectra strength of SCF and FCF-based probe, at the constant magnetic field. (b) CMS-scanned image shows the diameter of a humanoid fiber assembly. (c) Normalized plot to verify that the humanoid fiber structure is repeatable. (d) Comparison of the transmission intensities of nanomaterials-coated and uncoated optical fiber structure.

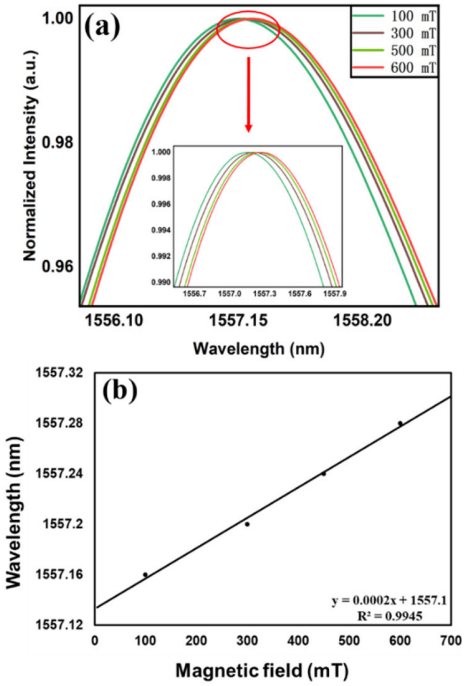

Fig. 10. Transmission spectra of an uncoated humanoid fiber structure with increasing magnetic field showing images of wave peak drift. (a) Sensing spectrum. (b) Linearity plot of magnetic field sensor.

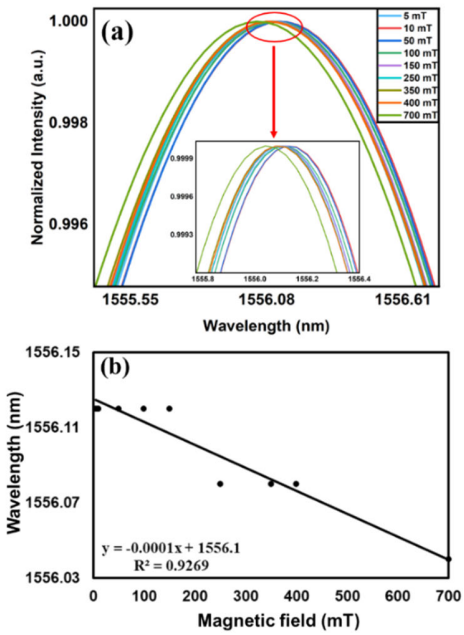

Fig. 11. Transmission spectra of an uncoated humanoid fiber structure with decreasing magnetic field showing images of wave peak drift. (a) Spectrum for sensing. (b) Linearity plot of magnetic field sensor.

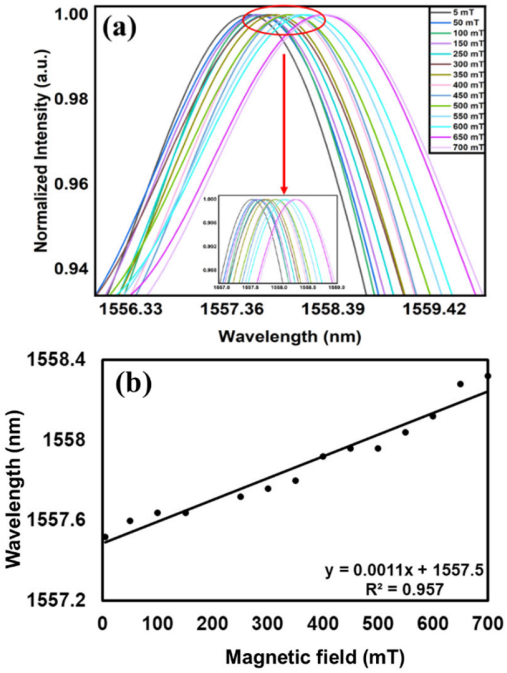

Fig. 12. Transmission spectra of coated humanoid fiber structure with increasing magnetic field showing images of wave peak drift. (a) Sensing spectrum. (b) Linearity plot of magnetic field sensor.

humanoid fiber structure in a decreasing magnetic field. Consequently, we want to coat the sensing region with $NiFe_2O_4$ to improve the sensor's sensing capability. The conditions of wave drift resulting from the reaction between the $NiFe_2O_4$ coated optical fiber and light leakage from the core in the detecting area of the humanoid fiber optic sensor into the cladding under the conditions of magnetic field enhancement and weakening are depicted in Figs. 12 and 13, respectively.

The normalized spectral images displayed in Figs. 12(a) and 13(a) clearly indicate the wavelength changes brought about by modifying the magnetic field strengths. When the magnetic field is increased, the fiber optic investigate, as seen in Fig. 12(b), exhibits a sensitivity of 1.1 pm/mT and an accuracy of 0.957; in contrast, the developed sensor investigate, as seen in Fig. 13(b), exhibits a sensitivity of 0.5 pm/mT and an accuracy of 0.9619 when the magnetic field is weakened. According to Figs. 12 and 13, it can be obtained that the

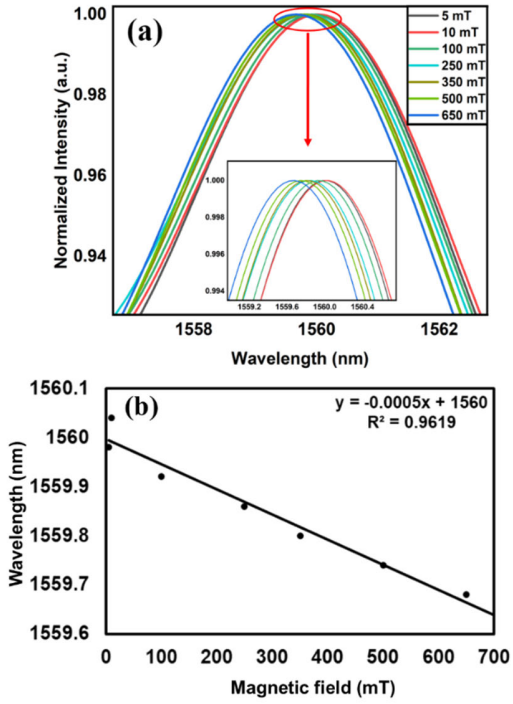

Fig. 13. Transmission spectra of coated humanoid fiber structure with decreasing magnetic field showing images of wave peak drift. (a) Sensing spectrum. (b) Linearity plot of magnetic field sensor.

slower or learning disability response of the wave deflection observed in decreasing magnetic fields compared to increasing magnetic fields is due to the hysteresis effect of the material. The hysteresis effect causes the material to retain a certain amount of magnetization after the removal or weakening of the external magnetic field, thus affecting the resonance behavior. It is also worth considering that the magnetic relaxation time of the material and the dynamics of particle alignment or reorientation under varying magnetic fields can also contribute to a slower or learning disability wave offset response.

The experiment's humanoid fiber optic sensors' sensing capabilities in rising and falling magnetic fields are displayed in Table I. The humanoid fiber optic sensors we looked at can measure up to 700 mT in both ascending and descending magnetic fields, according to the data in the graph. This sensor performs better in a rising magnetic field than it does in a decreasing magnetic field. The fiber optic structure has a sensitivity of 0.5 pm/mT in a decreasing magnetic field, whereas the humanoid fiber optic magnetic field sensor has a sensitivity of 1.1 pm/mT in an increasing magnetic field with an accuracy of 0.957. It is evident that humanoid fiber optic sensors function very well under magnetic fields that increase gradually.

The magnetic nanoparticles utilized in this stage of magnetic field detection are listed in Table II, along with a comparison of their magnetic field measurement ranges and detection efficiencies at various magnetic field strengths. We discovered that the $NiFe_2O_4$ employed in this experiment has a broader measuring range and higher sensitivity in the growing field compared to other nanoparticles by comparing the sensitivity and range of magnetic fields of other magnetic nanomaterials. In addition, it exhibits improved mobility within the current

TABLE I
COMPARISON OF THE SENSING PERFORMANCE OF HUMANOID FIBER OPTIC SENSORS IN ASCENDING AND DESCENDING MAGNETIC FIELDS

Specifications	Precursor sensing	Inverse sensing
Range of detection	0– 700 mT	0– 700 mT
Sensitivity	1.1 pm/mT	0.5 pm/mT
Accuracy	0.957	0.9619

TABLE II
COMPARING THE MAGNETIC FIELD SENSING CAPABILITIES WITH EXISTING MAGNETOFLUIDIC MATERIALS

Materials used	Sensing range	Sensitivity	Ref.
Magnetic fluid	40-150 GS	0.4325 nm/GS	[23]
Magnetic fluid	2-6 mT	−2370 pm/mT	[24]
$NiFe_2O_4$	0-700 mT	1.1 pm/mT	This Work

measurement range of magnetic fields. It is worth mentioning that in this work we measured the magnetic field strength based on the ferromagnetic effect of nickel compounds by coating the sensing region of the SMS fiber structure with $NiFe_2O_4$. The structural parameters of the SMS fiber structure were simulated by simulation experiments, during which the preparation of optical probes was attempted using three types of fiber fusion splicing, namely, SMF, MMF, and SCF. These operations greatly improved the repeatability of the fiber structure as well as the high sensitivity and accuracy.

IV. CONCLUSION

The development of a humanoid fiber optic sensor for magnetic field detection is the primary goal of this effort. The experimental findings demonstrate the exceptionally high manufacturing repeatability of our tapered fiber construction. We modified the humanoid fiber structure by applying $NiFe_2O_4$ coating to the fiber's detecting area to improve sensing performance. In the experiments that followed, we monitored the wavelength shift as the magnetic field strength changed. We found that the probe's linear fitting coefficients reached 0.957 and 0.9619 in the two scenarios, respectively, indicating that the humanoid fiber structure had a high sensitivity for accurately capturing the changing magnetic field trend. Note that this experiment only examined the magnetic field range of 0–700 mT due to limitations in the experimental apparatus. If the generator of magnetic fields is able to provide a stronger magnetic field, the sensor should continue to exhibit good stability. Consequently, the magnetic field sensor that is suggested in this study has a great deal of promise for use in the nonintrusive magnetic field measuring sector. Especially in the field of geological exploration and biomedical imaging, due to the characteristics of small size, high sensitivity, and high accuracy, this achievement will greatly ensure the accuracy of the detection results, and provide the feasibility of precise measurement of micro-magnetic fields in narrow spaces in the future.

REFERENCES

[1] C. Liu, T. Shen, H.-B. Wu, Y. Feng, and J.-J. Chen, "Applications of magneto-strictive, magneto-optical, magnetic fluid materials in optical fiber current sensors and optical fiber magnetic field sensors: A review," *Opt. Fiber Technol.*, vol. 65, Sep. 2021, Art. no. 102634, doi: 10.1016/j.yofte.2021.102634.

[2] A. Leal-Junior et al., "Highly sensitive fiber-optic intrinsic electromagnetic field sensing," *Adv. Photon. Res.*, vol. 2, no. 1, Jan. 2021, Art. no. 2000078, doi: 10.1002/adpr.202000078.

[3] J. Ma, H. Pei, H. Zhu, B. Shi, and J. Yin, "A review of previous studies on the applications of fiber optic sensing technologies in geotechnical monitoring," *Rock Mech. Bull.*, vol. 2, no. 1, Jan. 2023, Art. no. 100021, doi: 10.1016/j.rockmb.2022.100021.

[4] G. Yu et al., "Borehole seismic survey using multimode optical fibers in a hybrid wireline," *Measurement*, vol. 125, pp. 694–703, Sep. 2018, doi: 10.1016/j.measurement.2018.04.058.

[5] W. Lyu, W. Xu, F. Yang, S. Chen, F. Tan, and C. Yu, "Non-invasive measurement for cardiac variations using a fiber optic sensor," *IEEE Photon. Technol. Lett.*, vol. 33, no. 18, pp. 990–993, Sep. 15, 2021, doi: 10.1109/LPT.2021.3078757.

[6] D. Murzin et al., "Ultrasensitive magnetic field sensors for biomedical applications," *Sensors*, vol. 20, no. 6, p. 1569, Mar. 2020, doi: 10.3390/s20061569.

[7] D. J. Mapps, "Remote magnetic sensing of people," *Sens. Actuators A, Phys.*, vol. 106, nos. 1–3, pp. 321–325, Sep. 2003, doi: 10.1016/s0924-4247(03)00193-6.

[8] K. Jensen et al., "Magnetocardiography on an isolated animal heart with a room-temperature optically pumped magnetometer," *Sci. Rep.*, vol. 8, no. 1, p. 16218, Nov. 2018, doi: 10.1038/s41598-018-34535-z.

[9] H. Lee, T.-H. Shin, J. Cheon, and R. Weissleder, "Recent developments in magnetic diagnostic systems," *Chem. Rev.*, vol. 115, no. 19, pp. 10690–10724, Oct. 2015, doi: 10.1021/cr500698d.

[10] H. V. Thakur, S. M. Nalawade, S. Gupta, R. Kitture, and S. N. Kale, "Photonic crystal fiber injected with Fe_3O_4 nanofluid for magnetic field detection," *Appl. Phys. Lett.*, vol. 99, no. 16, Oct. 2011, Art. no. 161101, doi: 10.1063/1.3651490.

[11] G. Sharma, A. M. Shrivastav, A. Jana, and R. Jha, "Synthesized Fe_3O_4 nanoflowers coated microfiber as magnetometer," *IEEE Photon. Technol. Lett.*, vol. 30, no. 22, pp. 1925–1928, Nov. 2018, doi: 10.1109/LPT.2018.2872592.

[12] N. Alberto, M. Domingues, C. Marques, P. André, and P. Antunes, "Optical fiber magnetic field sensors based on magnetic fluid: A review," *Sensors*, vol. 18, no. 12, p. 4325, Dec. 2018, doi: 10.3390/s18124325.

[13] M. Alimohammadian and B. Sohrabi, "Observation of magnetic domains in graphene magnetized by controlling temperature, strain and magnetic field," *Sci. Rep.*, vol. 10, no. 1, p. 21325, Dec. 2020, doi: 10.1038/s41598-020-78262-w.

[14] S. Y. Yang, J. J. Chieh, H. E. Horng, C.-Y. Hong, and H. C. Yang, "Origin and applications of magnetically tunable refractive indexof magnetic fluid films," *Appl. Phys. Lett.*, vol. 84, no. 25, pp. 5204–5206, Jun. 2004, doi: 10.1063/1.1765201.

[15] A. Kumar, S. Sahu, and R. Jha, "Small angles vector magnetometer based on anisotropic ferromagnetic nanofluid functionalized fiber interferometer," *J. Phys. D, Appl. Phys.*, vol. 55, no. 40, Oct. 2022, Art. no. 405102, doi: 10.1088/1361-6463/ac7fc7.

[16] C. R. Taitt, G. P. Anderson, and F. S. Ligler, "Evanescent wave fluorescence biosensors: Advances of the last decade," *Biosensors Bioelectron.*, vol. 76, pp. 103–112, Feb. 2016, doi: 10.1016/j.bios.2015.07.040.

[17] W. Zhang et al., "Humanoid shaped optical fiber plasmon biosensor functionalized with graphene oxide/multi-walled carbon nanotubes for histamine detection," *Opt. Exp.*, vol. 31, no. 7, p. 11788, Mar. 2023, doi: 10.1364/oe.486844.

[18] Y. Zhao, D. Wu, R.-Q. Lv, and Y. Ying, "Tunable characteristics and mechanism analysis of the magnetic fluid refractive index with applied magnetic field," *IEEE Trans. Magn.*, vol. 50, no. 8, pp. 1–5, Aug. 2014, doi: 10.1109/TMAG.2014.2310710.

[19] N. Agrawal et al., "Detection of L-cysteine using silver nanoparticles and graphene oxide immobilized tapered SMS optical fiber structure," *IEEE Sensors J.*, vol. 20, no. 19, pp. 11372–11379, Oct. 2020, doi: 10.1109/JSEN.2020.2997690.

[20] X. Liu et al., "Plasmonic sensor based on offset-splicing and waist-expanded taper using multicore fiber for detection of aflatoxins B1 in critical sectors," *Opt. Exp.*, vol. 31, no. 3, p. 4783, Jan. 2023, doi: 10.1364/oe.479870.

[21] H. Yan, X. Song, X. Wang, and Y. Wang, "Electromagnetic wave absorption and scattering analysis for Fe_3O_4 with different scales particles," *Chem. Phys. Lett.*, vol. 723, pp. 51–56, May 2019, doi: 10.1016/j.cplett.2019.03.033.

[22] S. Khamari, A. Kumar, N. Mohapatra, and R. Jha, "$NiFe_2O_4$ ferrofluid to detect magnetic field using microfiber interferometry," *IEEE Sensors J.*, vol. 22, no. 5, pp. 4014–4021, Mar. 2022, doi: 10.1109/JSEN.2022.3142039.

[23] X. Yan et al., "Highly sensitive magnetic field sensors based on a D-type fiber with Bi_2O_2 Se film," *IEEE Sensors J.*, vol. 23, no. 24, pp. 30293–30301, Dec. 2023, doi: 10.1109/JSEN.2023.3326171.

[24] Y. Li et al., "All-fiber-optic vector magnetic field sensor based on side-polished fiber and magnetic fluid," *Opt. Exp.*, vol. 27, no. 24, p. 35182, Nov. 2019, doi: 10.1364/oe.27.035182.